Journal of the Korean Ceramic Society
Vol. 45, No. 11, pp. 675~680, 2008.

Characterization of Pore Structures for Porous Sintered Reaction-Bonded Silicon Nitrides with Varied Pore-Former Content

Young-Jo Park†, In-Hyuck Song, and Hai-Doo Kim

Engineering Ceramics Research Group, Korea Institute of Materials Science, Changwon 641-010, Korea
(Received November 4, 2008; Revised November 11, 2008; Accepted November 12, 2008)

ABSTRACT

The effect of pore former content on both porosity and pore structure was investigated for porous sintered reaction-bonded silicon nitrides (SRBSNs). A spherical PMMA with d_{50}=8 μm was employed as a pore-former. Its amount ranged from 0 to 30 part. Porous SRBSNs were fabricated by post-sintering at various temperatures where the porosity was controlled at 12~52%. The strong tendency of increasing porosity with PMMA content and decreasing porosity with sintering temperature was observed. Measured pore-channel diameter increased (0.3→1.1 μm) with both PMMA content and sintering temperature.

Key words : RBSN, SRBSN, Pore channel, Support, Filter, Separation

1. Introduction

In the past, ceramics research related to Si_3N_4 focussed on applications requiring strong and tough engineering parts. Since the early 1990's, some of this attention has been diverting away from conventional structural applications. In particular, and because of its planned usage as device substrates,[1-6] machinable ceramics,[7,8] and filtering media,[9-14] technological investigations focus on the enhancement of thermal conductivity and the development of porous structures. More specifically, crystallinity, texture, grain morphology, and pore size distributions are key.

By adjusting the characteristics of the sintering additives, such as the type and amount, used to obtain dense Si_3N_4 ceramics, porous Si_3N_4 ceramics have been realized through similar processes. Owing to their improved machinability, porous ceramic materials serve as excellent materials for industrial filtering applications. These include high-temperature gas filters, separation membranes, and catalyst supports; the acicular grain morphology found in these ceramics[15,16] makes them ideal candidates for filtering applications where filtering efficiency and permeability are essential. That is, the highly complex pore channel structure provided by the rod-like grains results in a large specific surface area that is efficient at trapping particulate matter (PM). Simultaneously, the large number of channels, compared to that of equiaxed-grained ceramics, compensates for clogging phenomena once filtering processes begin. Furthermore, Si_3N_4 ceramics offer the high thermal shock resistance and superior mechanical/chemical stability at high temperatures necessary for operations in high temperature and/or corrosive environments. Previously, porous Si_3N_4 ceramics research has focused on both strength sustainment of closed pore bodies[7,13,17-19] and microstructural evolution of whisker-like grains.[10-12]

In this research, metal silicon powder, which is less expensive than Si_3N_4 powder, was selected as a starting material. Reaction-bonding processes,[20-22] followed by post-sintering[23-27] were used to produce a porous Si_3N_4 support for a gas separation system. In general, supporting materials for gas separation applications are composed of large ceramic grains (20 μm average diameter) which makes them suitable mechanically strong and low gas-transport resistive materials. Until now, support materials have exclusively been alumina. Recently, the formation of SiC, SiCN, and Si_3N_4 (derived from preceramic polymers) membranes on alumina supports was investigated in an effort to address high-temperature environments.[28-30] However, there are incompatibility issues related to thermal expansion mismatch between Si based membranes and alumina support materials. Thus, in order to take advantage of non-oxide membranes, the development of compatible non-oxide support materials are crucial.

The goal of this research is to investigate the pore structures, such as porosity and pore channel size, in SRBSNs as a function of pore-former content and sintering temperature. Emphasis is placed on the establishment of processing route for the fabrication of a wide range of pore structures.

2. Experimental Procedure

A commercially available metal silicon powder was used in the present study (Sicomill grade 2, Vesta, Sweden; >98.6%, 0.4 wt.% Fe, 0.2 wt.% Al, d_{50}=7 μm). Commonly adopted oxide sintering additives, such as Y_2O_3 (grade C, H.

†Corresponding author : Young-Jo Park
E-mail : yjpark87@kims.re.kr
Tel : +82-55-280-3356 Fax : +82-55-280-3392

C. Stark, Germany; 99.99%, $d_{50}=0.7$ μm) and Al_2O_3 (AKP-30, Sumitomo, Japan; 99.99%, $d_{50}=0.31$ μm), were selected. The total amount of sintering additives was fixed at 2.3 wt%. The weight percentage of the sintering additives was calculated based on the amount of Si_3N_4 and assumed a perfect nitridation of raw silicon powder into Si_3N_4. Under this assumption, a weight gain of 66.5% was calculated. Spherical pore-formers (PMMA, Aldrich, $d_{50}=8$ μm) were blended in order to control both the pore structure and porosity of the sintered body. The amount of PMMA per 100 g of Si in the powder mixture was 0, 10, 20, and 30 g. These were designated as 0-part, 10-part, 20-part and 30-part, respectively.

Approximately 50 g of powder mixture (consisting of Si, sintering additives, and pore-former) was thoroughly milled in a nylon jar for 4 h; Si_3N_4 balls and ethanol were used as milling media. After drying the mixtures in a rotating evaporator, they were sieved to a particle size < 150 μm. The resulting powder mixture was uniaxially pressed into rectangular pellets measuring 10 mm × 10 mm × 2 mm. They were then cold isostatically pressed at 200 MPa. After shaping, the samples were heated up to 1350°C in a 95% N_2/5% H_2 flowing atmosphere using a horizontal tube furnace in which reaction-bonding occurred. Reaction times at 1350°C were 6 h for the 0 part mixture and 4 h for the others. A maximum of eight specimens were placed on a suspended BN-coated graphite plate. The specimens were placed upright (on their edges) and were out through a small hole in the graphite plate to minimize both contamination and temperature gradients. The percentage of nitridation was calculated from the weight change before and after the nitriding process. In preparation for the post-sintering of the nitrided specimens (RBSNs), samples taken from the nitriding furnace were placed in a BN-coated graphite crucible with Si_3N_4 powder filling its volume. Post-sintering was carried out in a graphite resistance furnace at 1700°C, 1800°C, and 1900°C for 2 h in a static nitrogen atmosphere (0.9 MPa). An SEM (Jeol, JSM-6700F, Japan) was used to observe the fracture surfaces, and X-ray diffraction (XRD, Rigaku, D/Max 2200, Japan) was used for phase identification. Pore size and distribution were characterized by Mercury prosimetry (Micromeritics, Autopore IV 9510, USA).

3. Results and Discussion

Due to small specimen size and uniform spring back in the regular rectangular shape, and in spite of difference in stiffness between the soft PMMA and the other hard components, crack-free sound green compacts were fabricated. Previously, the authors reported that a nitridation rate of in excess of 90% usually results in no residual Si for 20-part PMMA specimens when they are nitrided at 1350°C for 4 h.[31] The same nitriding conditions employed for the 10-part, 20-part, and 30-part specimens in this research yielded similar nitridation rates. Owing to the relatively poor accessibility of the nitriding gas, which was caused by

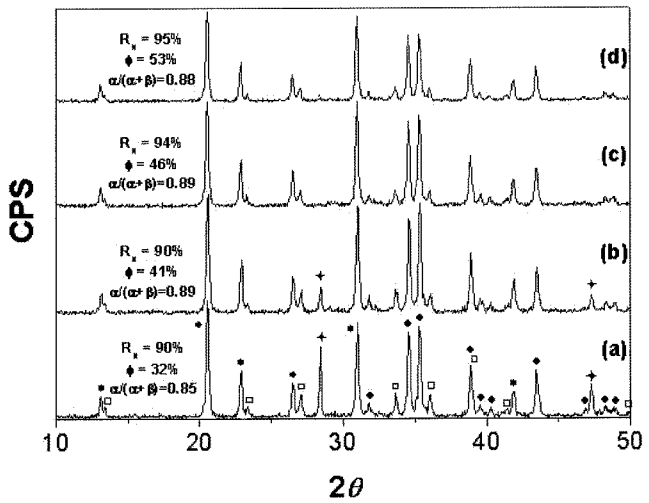

Fig. 1. XRD analysis of RBSNs nitrided at 1350°C. (a) 0 part, (b) 10 part, (c) 20 part, (d) 30 part. α-Si_3N_4 (●), β-Si_3N_4 (□), Si (+).

relatively dense compaction, for the 0-part specimen, increasing nitriding time (up to 6 h) was necessary in order to boost the nitridation rate close to 90%. XRD patterns of the nitrided specimens indicate an increase in both nitridation rate and porosity with PMMA content (Fig. 1 -nitridation rate (R_N), porosity (ϕ), and α-Si_3N_4 fractions are shown in the inset). An α-Si_3N_4 phase formed predominantly via current nitriding reaction, which is well known tendency for a nitriding of silicon mixture. Unreacted residual Si was detected in both the 0-part and 10-part specimens. Since the residual Si is completely nitrided during the subsequent post-sintering process, deterioration of properties (at service conditions) caused by this residual Si can be excluded.

Fig. 2 depicts the fracture morphology of the as-nitrided specimens from Fig. 1. Raw Si particles ($d_{50}=7$ μm) were transformed into Si_3N_4 particles of a few hundred nanometers in size. Whisker-like grains are found mainly around both the original open spaces in the powder compacts and open spaces resulting from decomposition of PMMA. Post-sintering at elevated temperatures gave rise to a typical rod-like microstructures β-Si_3N_4 grains (Fig. 6(c),(d)).

Porosity and shrinkage of the post-sintered specimens was investigated (Fig. 3 and 4, respectively). As pointed out in the last section, raw Si and α-Si_3N_4 phases are completely transformed into the β-Si_3N_4 phase in all the SRBSNs (Fig. 7). Porosity of the nitrided specimens (RBSNs) is plotted for comparison in Fig. 3; RBSN shrinkage values were not included in Fig. 4 as they are virtually zero. Porosity decreased monotonically from that of RBSNs with increase in sintering temperatures, while increase in porosity at the same sintering temperature is proportional to blended PMMA content. The observation of increased shrinkage with sintering temperatures (Fig. 4) is directly related to decreased porosity (Fig. 3). On the other hand, it is interesting to note that nearly constant shrinkage was measured at the same sintering temperature for samples with varied

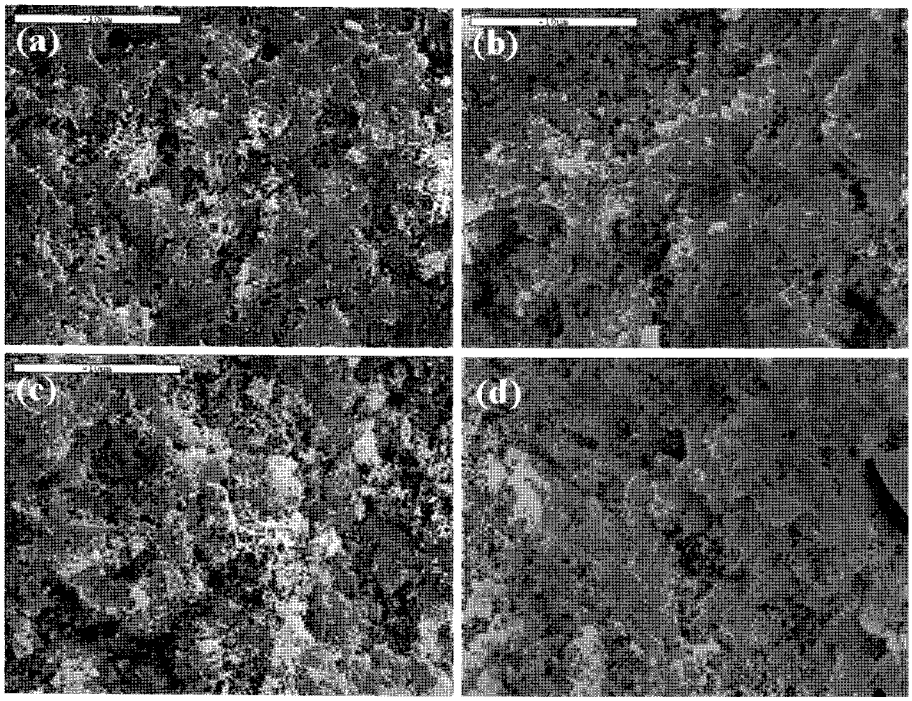

Fig. 2. SEM micrographs of fracture surfaces of RBSNs nitrided at 1350°C. (a) 0 part, (b) 10 part, (c) 20 part, (d) 30 part.

PMMA content.

Grain morphology and pore structure of the post-sintered specimens were observed on the fracture surface. Fig. 5 shows the porous microstructures of SRBSNs sintered at 1900°C for 2 h with varied PMMA content. Larger grain growth with increases in PMMA content is attributed to the increased abundance of open space thus allowing grains to grow for a longer time before grain-impingement halts growth. Substantial grain growth is seen with increase in sintering temperatures (Fig. 6). Typical rod-like grain morphology of β-Si_3N_4 ceramics is peculiar from the sintering at 1800°C (Fig. 6(c),(d)). XRD analyses indicate that complete phase transformation into β-Si_3N_4 phase occurred at 1700°C (Fig. 7). Therefore, the evolution of rod-like grains from the equiaxed grains are mainly attributable to solution-reprecipitation of the β-Si_3N_4 phase. Herein, rapid phase transformation is rationalized with a smaller amount of sintering additive in the current research. That is, the short diffusion distance resulting from the smaller liquid phase content promoted the kinetics of phase transformation.

Pore-channel size as a function of PMMA content and sintering temperature was measured using a mercury porosimeter (Fig. 8). Channel size increased substantially from that of RBSNs via post-sintering (Fig. 2). The mean pore size of RBSNs is less than 500 nm due to the fine size of the as-nitrided particles, while those of SRBSNs range from 0.3-

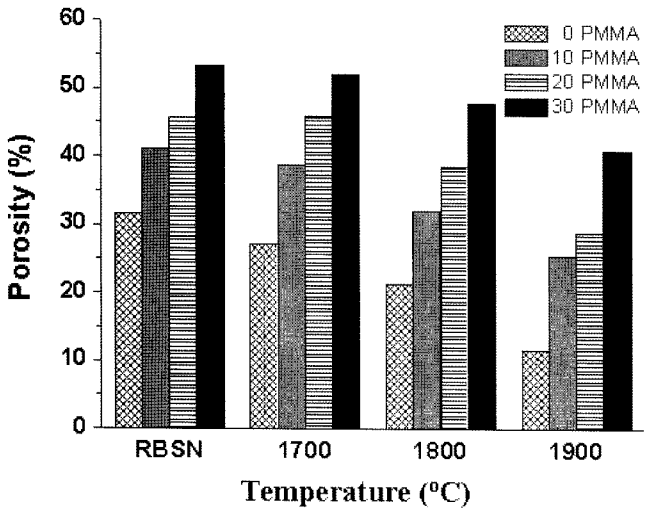

Fig. 3. Measurement of porosity of SRBSNs post-sintered at various temperatures.

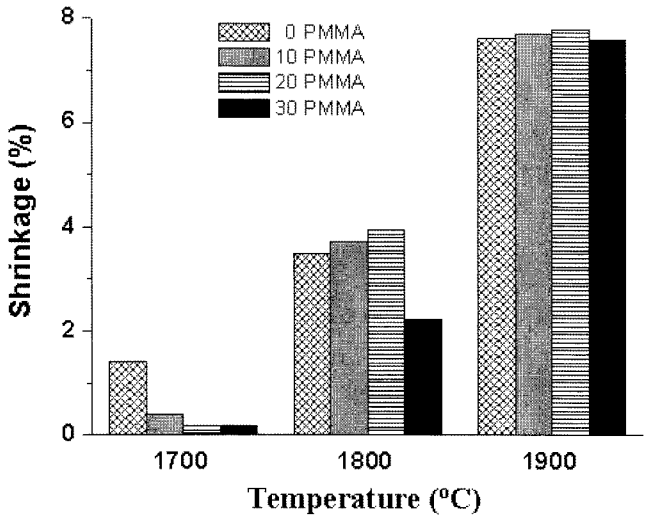

Fig. 4. Measurement of shrinkage of SRBSNs post-sintered at various temperatures.

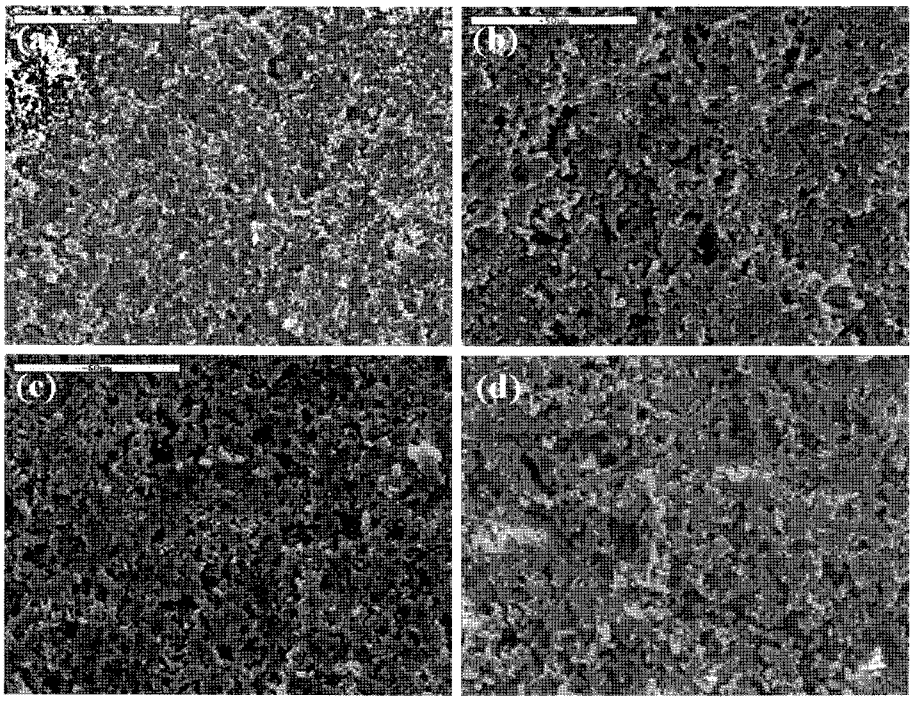

Fig. 5. SEM micrographs of fracture surface of SRBSNs post-sintered at 1900°C for 2 h. (a) 0 part, (b) 10 part, (c) 20 part, (d) 30 part.

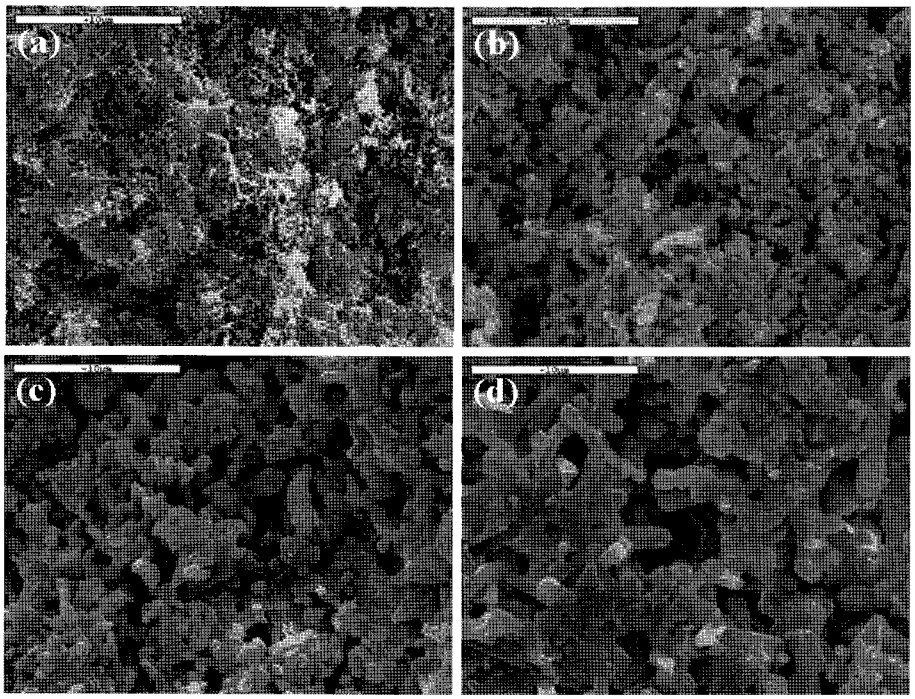

Fig. 6. SEM micrographs of fracture surface of 20 part RBSN and SRBSNs post-sintered at various temperatures. (a) RBSN, (b) 1700°C, (c) 1800°C, (d) 1900°C.

1.1 μm. Pore size increases with both sintering temperature and PMMA content. Noteworthy is the increase in pore diameter with sintering temperature. Increase in pore diameter with sintering temperature is odd, because total porosity decreased by post-sintering owing to increased shrinkage (Fig. 3). While it has been shown that the sintering of ceramics induces pore growth in the course of grain growth. That is, effective pore diameters increase by the sintering process as a consequence of the coalescence of pores.

4. Conclusions

A cost-effective fabrication route of porous supports for membranes was successfully developed by nitriding and

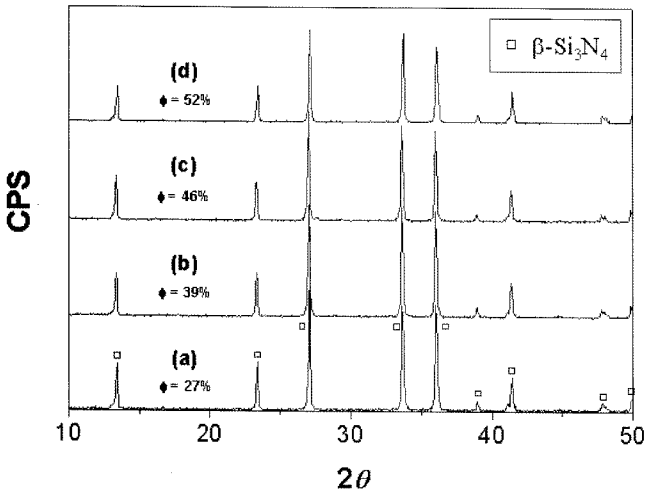

Fig. 7. XRD analysis of SRBSNs post-sintered at 1700°C for 2 h. (a) 0 part, (b) 10 part, (c) 20 part, (d) 30 part. In the figure, ϕ stands for the porosity.

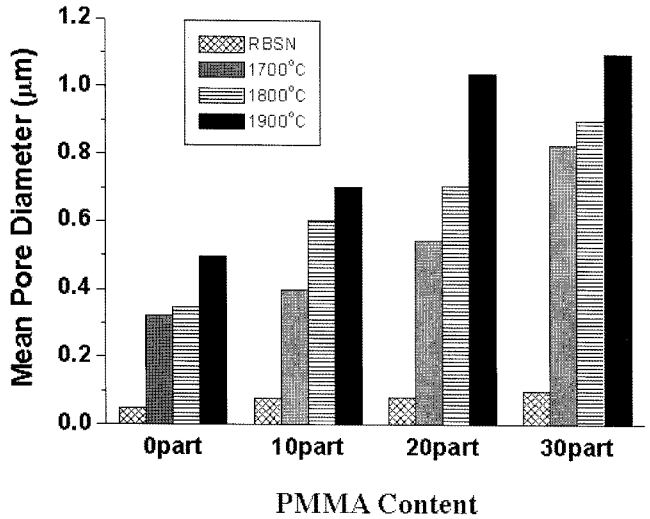

Fig. 8. Measurement of pore channel size of SRBSNs post-sintered at various temperatures.

post-sintering of Si mixtures. The variation in pore-former content and sintering time resulted in a wide range of pore channel sizes as well as total porosity. At present, there is no optimum porosity and pore size desirable for support of gas separation systems. SRBSNs in the present research covered total porosity from 12~53% and mean pore diameters from 0.3 to 1.1 μm. Considering the merit of near-net shaping capability and cost effectiveness of porous SRBSNs, engineering implications of the current research are clear.

REFERENCES

1. M. Kitayama, K. Hirao, M. Toriyama, and S. Kanzaki, "Thermal Conductivity of β-Si_3N_4: I, Effects of Various Microstructural Factors," *J. Am. Ceram. Soc.*, **82** [11] 3105-12 (1999).
2. M. Kitayama, K. Hirao, A. Tsuga, K. Watari, M. Toriyama, and S. Kanzaki, "Thermal Conductivity of β-Si_3N_4: II, Effect of Lattice Oxygen," *J. Am. Ceram. Soc.*, **83** [8] 1985-92 (2000).
3. M. Kitayama, K. Hirao, K. Watari, M. Toriyama, and S. Kanzaki, "Thermal Conductivity of β-Si_3N_4: III, Effect of Rare Earth (RE=La, Nd, Gd, Y, Yb and Sc) Oxide Additive," *J. Am. Ceram. Soc.*, **84** [2] 353-58 (2001).
4. K. Watari, K. Hirao, M. E. Brito, M. Toriyama, and S. Kanzaki, "Hot Isostatic Pressing to Increase Thermal Conductivity of Si_3N_4 Ceramics," *J. Mater. Res.*, **14** [4] 1538-41 (1999).
5. H. Yokota and M. Ibukiyama, "Microstructure Tailoring for High Thermal Conductivity of β-Si_3N_4 Ceramics," *J. Am. Ceram. Soc.*, **86** [1] 197-99 (2003).
6. N. Hirosaki, Y. Okamoto, F. Munakata, and Y. Akimune, "Effect of Seeding on the Thermal Conductivity of Self-reinforced Silicon Nitride," *J. Euro. Ceram. Soc.*, **19** 2183-87 (1999).
7. C. Kawai and A. Yamakawa, "Effect of Porosity and Microstructure on the Strength of Si_3N_4: Designed Microstructure for High Strength, High Thermal Shock Resistance, and Facile Machining," *J. Am. Ceram. Soc.*, **80** [10] 2705-08 (1997).
8. J. F. Yang, Z. Y. Deng, and T. Ohji, "Fabrication and Characterization of Porous Silicon Nitride Ceramics Using Yb_2O_3 as Sintering Additive," *J. Euro. Ceram. Soc.*, **23** 371-78 (2003).
9. N. Miyakawa, H. Sato, H. Maeno, and H. Takahashi, "Characteristics of Reaction-bonded Porous Silicon Nitride Honeycomb for DPF Substrate," JSAE Review, **24** 269-76 (2003).
10. C. Kawai and A. Yamakawa, "Network Formation of Si_3N_4 Whiskers for the Preparation of Membrane Filters," *J. Mater. Sci. Lett.*, **17** 873-75 (1998)
11. C. Kawai and A. Yamakawa, "Crystal Growth of Silicon Nitride Whiskers through a VLS Mechanism Using SiO_2-Al_2O_3-Y_2O_3 Oxides as Liquid Phase," *Ceram. Int.*, **24** 135-38 (1998).
12. C. Kawai, T. Marsuura, and A. Yamakawa, "Separation-Permeation Performance of Porous Si_3N_4 Ceramics Composed of β-Si_3N_4 Grains as Membrane Filters for Microfilteration," *J. Mater. Sci.*, **34** 893-96 (1999).
13. J. F. Yang, G. J. Zhang, and T. Ohji, "Fabrication of Low-shrinkage, Porous Silicon Nitride Ceramics by Addition of a Small Amount of Carbon," *J. Am. Ceram. Soc.*, **84** [7] 1639-41 (2001).
14. D. Chen, B. Zhang, H. Zhuang, and W. Li, "Combustion Synthesis of Network Silicon Nitride Porous Ceramics," *Ceram. Int.*, **29** 363-64 (2003).
15. M. Kramer, M. J. Hoffmann, and G. Petzow, "Grain Growth Kinetics of Si_3N_4 during α/β-transformation," *Acta Metall. Mater.*, **41** [10] 2939-47 (1993).
16. A. J. Pyzik and D. R. Beaman, "Microstructure and Properties of Self-reinforced Silicon Nitride," *J. Am. Ceram. Soc.*, **76** [11] 2737-44 (1993).
17. C. Kawai, "Effect of Grain Size Distribution on the Strength of Porous Si_3N_4 Ceramics Composed of Elongated β-Si_3N_4 Grains," *J. Mater. Sci.*, **36** 5713-17 (2001).
18. Y. Inagaki, N. Kondo, and T. Ohji, "High Performance

Porous Silicon Nitrides," *J. Euro. Ceram. Soc.*, **22** 2489-94 (2002).
19. N. Kondo, Y. Inagaki, Y. Suzuki, and T. Ohji, "Fabrication of Porous Anisotropic Silicon Nitride by Using Partial Sinter-forging Technique," *Mater. Sci. Eng.*, **A335** 26-31 (2002).
20. A. J. Moulson, "Reaction-bonded Silicon Nitride: its Formation and Properties," *J. Mater. Sci.*, **14** 1017-51 (1979).
21. H. M. Jennings, "On Reactions between Silicon and Nitrogen," *J. Mater. Sci.*, **18** 951-67 (1983).
22. G. Ziegler, J. Heinrich, and G. Wotting, "Relationships between Processing, Microstructure and Properties of Dense and Reaction-bonded Silicon Nitride," *J. Mater. Sci.*, **22** 3041-86 (1987).
23. A. Giachello and P. Popper, "Post-sintering of Reaction-bonded Silicon Nitride," *Ceram. Inter.*, **5** [3] 110-14 (1979).
24. J. A. Mangles and G. J. Tennenhouse, "Densification of Reaction-bonded Silicon Nitride," *J. Am. Ceram. Soc. Bull.*, **59** 1216-19 (1980).
25. H. J. Kleebe and G. Ziegler, "Influence of Crystalline Second Phases on the Densification Behavior of Reaction-bonded Silicon Nitride during Post Sintering under Increased Nitrogen Pressure," *J. Am. Ceram. Soc.*, **72** [12] 2314-17 (1989).
26. B. T. Lee, J. H. Yoo, and H. D. Kim, "Size Effect of Raw Si Powder on Microstructures and Mechanical Properties of RBSN and GPSed-RBSN Bodies," *Mater. Sci. Eng.*, **A333** 306-13 (2002).
27. X. Zhu, Y. Zhou, and K. Hirao, "Post-densification Behavior of Reaction-bonded Silicon Nitride (RBSN): Effect of Various Characteristics of RBSN," *J. Mater. Sci.*, **39** 5785-97 (2004).
28. H. Suda, H. Yamauchi, Y. Uchimaru, I. Fujiwara, and K. Haraya, "Preparation and Gas Permeation Properties of Silicon Carbide-based Inorganic Membranes for Hydrogen Separation," *Desalination*, **193** 252-55 (2006).
29. Y. Iwamoto, K. Sato, T. Kato, T. Inada, and Y. Kubo, "A Hydrogen-permselective Amorphous Silica Membrane Derived from Polysilazane," *J. Euro. Ceram. Soc.*, **25** 257-64 (2005).
30. Z. Li, K. Kusakabe, and S. Morooka, "Preparation of Thermostable Amorphous Si-C-O Membrane and its Application to Gas Separation at Elevated Temperature," *J. Membr. Sci.*, **118** 159-68 (1996).
31. Y. J. Park, E. Choi, H. W. Lim, and H. D. Kim, "Design of Porosity Level for Porous Si_3N_4 Ceramics Manufactured by Nitriding and Post-sintering of Si Powder Compact," *Mater. Sci. Forum*, **534-536**, 1017-20 (2007).